STEEL: COUPLED INFLUENCE OF THE INITIAL METALLURGICAL STATE AND THE HEATING RATE

N. Zavaleta Gutiérrez[1], M. I. Luppo[2], C. A. Danon[2], I. Toda-Caraballo[3,4], C. Capdevila[3*] and C. García de Andrés[3]

[1] Engineering Faculty; Mining and Metallurgy Department, Av. Juan Pablo II s/n, Trujillo National University, Peru

[2] National Commission of Atomic Energy, Materials Department Av. Gral. Paz 1499, 1650 San Martín, Buenos Aires, Argentina.

[3] MATERALIA Research Group, Physical Metallurgy Department Centro Nacional de Investigaciones Metalúrgicas (CENIM), Consejo Superior de Investigaciones Científicas (CSIC) Avda. Gregorio del Amo, 8. E-28040 Madrid, Spain

[4] Dept. Materials Science and Metallurgy, University of Cambridge, Pembroke Street, Cambridge, CB2 3QZ, United Kingdom

[*] Corresponding author: ccm@cenim.csic.es

Abstract

The coupled influence of the initial metallurgical state and the heating rate to austenite on the occurrence of heterogeneous grain growth during austenitization of an ASTM A213 – T91 steel has been studied. To that aim, two-step thermal cycles were designed. In the first step, different starting metallurgical conditions were obtained by treating the as-received material at 780 °C for increasing times up to 6 hours. In the second step, “in situ” austenitization was performed by heating to austenite at rates of 1, 30 and 50 ºC/s and then holding at 1050 ºC for 30’.

Two types of austenite grain structures were obtained after austenitization, namely, homogeneous and heterogeneous. The homogeneous structure was characterized by a smooth size distribution of approximately equiaxed, normally grown grains. The heterogeneous structure, instead, exhibited the exaggerated growth of a few austenite grains embedded in a small to medium-sized “matrix”.

For the 1 ºC/s heating rate and all of the initial metallurgical states, only homogeneous grain growth was observed, whereas for the 50 ºC/s heating rate only heterogeneous grain growth was observed regardless the starting metallurgical condition. Instead, the occurrence of homogeneous or heterogeneous grain growth after heating at 30 ºC/s was observed to be a function of the time of previous tempering. Some explanations of the phenomenon are advanced taking into account the precipitation state of second phases.

Keywords: T91 steel, austenitization, heating rate, grain growth

1. Introduction

Ferritic-martensitic steels of the 9%Cr1%Mo type have been extensively used in conventional and nuclear power plant components, heat exchangers, piping and tubing, etc., due to an excellent combination of properties such as creep resistance, toughness and resistance to oxidation at high temperatures [1- 3]. The continuous improvement of the properties of 9%Cr steels in the last decades has allowed a substantial increment of their benefits: increase of the service temperatures -with the consequent increase in efficiency- and increasingly important values of resistance to rupture [4- 6]. From the environmental point of view, the increase of the efficiency also implies a reduction of CO_2 emissions.

Austenite grain growth is theoretically explained taking as a basis the model proposed by Zener[7], which has been adapted for non-equilibrium kinetics, taking into account the experimental evidence that during a isothermal and/or continuous heating, the amount of microalloyed and interstitial (carbon and nitrogen) elements in austenite solid solution is altered and different from that predicted by the solubility product. Microalloying elements like vanadium, niobium and titanium are employed to produce fine precipitation in the matrix. The austenite grain boundaries and dislocations are pinned by these precipitates, inhibiting their movement during the thermal and thermomechanical processing of steels. This pinning force is governed by the thermodynamic stability of second-phase precipitates in austenite[8-9]. The temperature at which the equilibrium existing between driving forces for grain growth and pinning is broken, is defined as the grain coarsening temperature. At this temperature abnormal grain growth begins and a nonuniform grain microstructure is obtained [10].

Heterogeneous or abnormal grain growth in austenite may be a non-wished result of manufacturing processes implying austenitization. The mechanical properties of materials displaying a bimodal austenite grain size distribution could be degraded, and some examples of such a situation have been already reported [11- 13] Thus, it is important to control the thermal cycle parameters in processes requiring stages of austenite holding so as to avoid heterogeneities in grain size. In this sense, the influence of the heating rate (V_H) to austenite in the austenitic grain

size distribution -particularly, in the formation of a heterogeneous grain size structure- has been reported in the literature referred to carbon steels [7,14], microalloyed steels containing Ti, and V and Nb [8-1110,15,18], ferritic-martensitic 9% Cr [19- 21] and martensitic 14% Cr [22] steels. In some cases, a critical value for the heating rate has been found, above which a heterogeneous austenite grain size distribution is developed for fixed conditions of austenite temperature and holding time [20,23]. Thus, the heating rate to austenite and the austenitization temperature, T_A, would play a role on heterogeneous grain growth through their influence on the volume fraction and size of precipitates, which in turn would lead to local variations of the austenite grain size. At the same time, it should be kept in mind that though the action of pinning of the austenitic grain boundaries is exerted by carbides, nitrides or carbonitrides of the form MX (M=Nb,V; X=C,N), the major precipitated phase in T91 type steels in the as-received condition is constituted by carbides of the form $M_{23}C_6$ (M=Cr,Fe), whose dissolution during heating or austenite holding could also influence the kinetics of precipitation/dissolution of the MX *via* the increment of the C content in solid solution.

The present investigation aims to study the influence of the initial metallurgical state and the heating rate to austenite on the development of a heterogeneous austenite grain size distribution at temperatures normally used in industrial practice. To this end, two-step thermal cycles (i.e., thermal treatment at 780 ºC and “in situ” further austenitization) were designed and carried out in a high temperature, high resolution quenching dilatometer. The dilatometric response recorded along the second step of the thermal cycle, i.e., the austenitization process, provided qualitative evidences about the changes in chemical composition that austenite would undergo during its formation process. The precipitation state of second phases that exists at the austenitization temperature of 1050 °C, which is reached after the different thermal cycles tested, is also analyzed.

2. Materials and experimental procedure

A tube (8 mm wall-thickness) of ASTM A213 grade T91 steel was provided by V&M (France) in the normalized and tempered condition, i.e; austenitized at 1060 °C, 20 min. and tempered at 780 °C

for 40 min. The chemical composition of the steel is shown in Table 1. The composition of the Nb-free, V-free ASTM A213 grade T9 steel used in the present investigation for comparison purposes is also shown in Table 1.

The reverse transformation (tempered martensite $\rightarrow$ austenite) was followed by high resolution dilatometry. Experiments were performed with an Adamel-Lhomargy DT1000 quench dilatometer described elsewhere [24]. Samples were cylinders 12 mm-long and 3 mm in diameter. All samples were machined following the rolling direction of the tube.

Two-step thermal cycles were designed in order to assess the coupled influence of the initial metallurgical state and the heating rate to austenite on austenite grain growth. Thus, samples were heated to the industrial tempering temperature (780 ºC) at 5 ºC/s, held at that temperature for increasing times and then austenitized at 1050 ºC for 30 min. Times for heat treatment at 780 ºC were chosen so as to accumulate 1 to 6 hours by addition of the factory (40 min) and laboratory tempering times respectively. Heating rates to austenite were 1, 30 and 50 ºC/s. After austenitizing, samples were quenched at 50 ºC/s to room temperature applying a cold-He jet. Temperature ramps and isothermal holding steps were performed under primary vacuum of 1Pa; a scheme of the complete thermal cycle is shown in Figure 1. The dilatometric behavior of the samples during thermal cycles was acquired and recorded as a function of temperature and time in every case.

After thermal cycles, samples were tempered in order to promote the precipitation of $M_{23}C_6$ carbide particles at prior austenite grain boundaries; they were then embedded in a resin, grounded so as to expose the mid plane, polished down to 1 µm diamond cloth and etched with an oxalic acid reagent to be examined by optical microscopy. A combined technique of successive steps of polishing and etching was applied to distinguish the prior austenite grain boundaries in the tempered martensite structure. This made possible to obtain readily a qualitative picture of the austenitic grain structure.

The austenite grain size distribution of each sample was determined by image analysis following the ASTM E112-10 procedure [25]. A sketch of austenite grain boundaries was obtained in every case from the optical metallographic images and then treated with a software package. Equivalent grain diameters were obtained by averaging grain radii taken from the centroid of each grain at

intervals of 2 degrees. In this way, a mean grain diameter and area were obtained for every grain in the sample. ASTM grain areas and sizes were measured and classified as well. Approximately two to five thousand grains were counted in each sample. For the sake of comparison, exactly the same thermal cycles were repeated for selected values of the tempering time and heating rate to austenite for the T9 steel.

Extractive replicas of the heat-treated samples were prepared by C evaporation and further etching with the Villela reagent in the case of the series of T91 samples heated to austenite at 30 ºC/s. The chemical composition of precipitated phases was measured on these replicas in a Phillips CM200 TEM, operated at 200 kV and attached with an EDAX-DX4 system for energy-dispersive analysis of X-rays (EDS). 50 to 60 particles were measured in each sample.

3. Results

3.1 Austenite grain size distributions

Grain diameter histograms were constructed with the experimental data taken from each of the tested samples. Bin sizes were chosen according to grain size data as 2.5 μm for the T91 steel and 5 μm for the T9 steel respectively. The experimental grain diameter histograms were fitted to a lognormal distribution in every case; the results are shown in Figures 2, 3 and 4 for the samples of the T91 steel austenitized at 1, 30 and 50 ºC/s respectively. In each case, the corresponding optical micrograph illustrating the prior austenite grain structure is also shown. In the case of the 1 ºC/s heating rate, only homogeneous austenite grain size distributions were obtained. In the case of the 30 and 50 ºC/s heating rates, heterogeneous or homogeneous grain growth was observed as a function of the time in the tempering step. For the sake of clarity, the complete set of results is summarized in Table 2.

It turns out to be clear that, in the conditions given in Table 2, a few abnormal grains grow in a small-sized austenite grain matrix after 30 minutes of austenite holding at 1050 ºC. The results also suggest that the number of abnormal grains is a decreasing function of the time of treatment at 780 ºC before the austenitizing step. On the other hand, the parameters characterizing the lognormal size distribution of the “normal” (i.e, small to medium sized) grain population remain remarkably constant as a function of the time elapsed at 780 ºC.

The austenite grain size distribution of the T9 steel doesn't display this striking feature, although the mean grain size of the T9 steel is, as expected, larger than the T91 one; these features are displayed in Figures 5 and 6 along with the corresponding grain diameter histograms.

The comparison of the behavior of the two steels would indicate that the origin of the abnormal growth must be sought not only in the microstructural state of the tempered martensite immediately before austenitizing –that plays a role on the nucleation and growth of austenite- but also in the microstructure at the end of holding time (30 min) at the austenitization temperature (1050 ºC), i.e. the existence of second-phase precipitates, since the T9 steel is free of stabilizing alloying elements such as V and Nb.

3.2 Dilatometric record of the austenitization process.

Figure 7 shows the dilatometric curves that account for the transformation to austenite during heating of the T91 and T9 steels when the heating rate is settled at 1, 30 and 50 ºC/s and the initial metallurgical state is the as-received one. As expected, the higher the heating rates, the more the temperatures A_{c1} and A_{c3} are shifted to higher values [26-31]. At the same time, for the 30 and 50 ºC/s cases, there is a clear change of slope in the intercritical portion of the curve at temperatures in the region of 900-925 ºC, suggesting that the transformation to austenite proceeds with two distinct regimes. These two distinct regimes are not apparent when the applied heating rate is 1 ºC/s.

Figure 8 shows the comparison of the dilatometric curves accounting for heating at 1, 30 and 50 ºC/s from different tempering stages at 780 °C in T91and T9 steels. The transformation temperatures A_{c1} and A_{c3} seem to be weakly affected by the tempering time when heating is performed at 1ºC/s (Figure 8(a)) in T91 steel. On the other hand, it is clear from Figure 8(c) that the tempering time does markedly affect the shape and critical temperatures of the austenite transformation curves when heating is performed at 50 ºC/s; an incipient, intermediate behavior is evidenced at 30 ºC/s (Figure 8(b)). The transformation temperatures A_{c1} and A_{c3}, along with the transformation temperature interval, are summarized in Figure 9.

At all the heating rates tested in T91 steel, the values of the A_{c1} temperature show an increment with the time of previous tempering at 780 ºC when compared to the corresponding to the as-received material (Figure 9); this trend becomes even more evident for the T9 alloy. In both cases, the A_{c1} increment can be safely attributed to a metallurgical effect and not to the experimental error. In contrast, the evolution of A_{c3} temperature with the previous tempering time changes depending on heating rate. In this sense, for the T91 steel, an increase of A_{c3} for V_H=1 °C/s is recorded. However a significant decrease of A_{c3} is detected if V_H is raised to 30 °C/s. Finally, a flat trend is detected for heating at 50 °C/s. The latter is not detected in T9 steel where a significant increase in A_{c3} is recorded for V_H = 50 °C/s.

3.3 Chemical composition of precipitated phases after thermal cycles

Figure 10 illustrates an example of the observed precipitates after, respectively, tempering of martensite at 780 ◦C and tempering + austentization for the T91 steel. With regard to the issue of tempering, it is worth to mention that a thorough study of the stability of carbide phases with respect to size and composition during the thermal treatment at 780 ºC has been published elsewhere [32]; the major carbides were found to be, by far, the $M_{23}C_6$-type ones. On the other hand, the MX-type carbides or carbonitrides were classified in three subtypes (I, II and III) according their morphology and chemical composition: type I were spheroidal or cuboidal-like and Nb-rich, type II were plate-like and V-rich, and type III displayed the so-called “wing” morphology, with a Nb-rich core and V-rich “wings”. A subset of “wing” precipitates tend to coarsen during tempering meanwhile other are dissolved. As reported previously, in the case in which MX with a V-rich “wing” precipitate in the matrix, niobium carbonitride precipitates first as core and vanadium carbonitrides precipitate continuously on the core [32,33].

Figure 11 shows the chemical composition –only as for metallic elements- of the phases precipitated after the complete thermal cycle in a Cr-Nb-V ternary diagram, as measured by TEM-EDS analyses. The results correspond to the series of samples heated to austenite at a rate of 30 ºC/s, and determined that precipitates are MX-type carbonitrides. Composition measurements are

clearly located around Nb-rich values, in agreement with previous results indicating that Nb-rich phases are the only stable ones in austenite at high temperatures [34]. However, even considering that the size of the particle sample taken in each case could bias the obtained results, an incipient trend is observed in Figure 11 that indicates a V enrichment of the precipitated phases after the complete thermal cycle when the time in the tempering step is increased.

4. Discussion

The observations in Section 3.3 above serve as starting point to discuss the whole set of obtained results. In providing a framework for the analysis of heterogeneous austenite grain growth, one of the key ideas is to contrast the chemical composition of second-phase MX precipitates -which play a main role in inhibiting austenite grain growth by pinning grain boundaries- measured in this work after treating samples at 1050 ºC, against that reported at 780 ºC for the major MX particles. The major MX group at 780 ºC is constituted by V-rich (Type II) particles [32], which means that, taking into account the complete thermal cycle shown in Fig. 1 (tempering at 780 ºC + austenitization at 1050 ºC) *there is a change in the chemical identity of the major MX particles, from V-rich at 780 ºC to Nb-rich at 1050 ºC, during the heating ramp and/or austenite holding*. In addition, it is likely that the observed shift in the austenite transformation temperatures -that appears as a consequence of the increase in the heating rate- results in changes of the chemical composition of the initially formed austenite.

According to previously reported equilibrium thermodynamic calculations [35], the completion of $M_{23}C_6$ dissolution in austenite in the two steels studied (T91 and T9) occurs slightly above their respective A_{c3} temperatures; thus, considering in addition the influence of kinetic factors associated with the non-equilibrium heating conditions, we can assume that the dissolution of $M_{23}C_6$ carbides will be completed during the heating ramp or austenite holding at 1050 °C. Taking into account the cooling rate used in the present work (50 ºC/s), we can also assume that the precipitation state of carbide phases obtained after the final quenching is, to a very good approximation, representative of the one existing at high temperature, i.e., 1050 ºC. This implies, in turn, to assume that the only

precipitated phase to be found in the as-quenched condition of the T91 steel is constituted by MX-type carbides or mixed carbonitrides (M = Cr, Nb, V; X = C, N). This assumption follows from the fact that the $M_{23}C_6$ carbides existing in the as-tempered state are dissolved during austenite holding and will not precipitate during quenching and also by noting that the solvus temperature of MX-type carbides or carbonitrides is significantly higher than that of $M_{23}C_6$ carbides [31]. Since the T9 steel cannot form MX-type carbonitrides, there will be no carbides present in its as-quenched condition.

4.1 Coupling of the thermal cycle parameters and heterogeneous austenite grain growth

4.1.1 Isothermal holding at 780 ºC and austenite transformation temperatures

The relationship between the transformation temperatures A_{c1} and A_{c3} and the chemical composition of steels has been widely studied both by means of thermodynamic calculations [36] and empirical equations successfully proposed [37-39]. The experimental results of Figures 7 and 8 show that the holding time in the isothermal treatment at 780 °C could have a non-negligible influence on the chemical composition of the formed austenitic phase, since the start and finish transformation temperatures, A_{c1} and A_{c3}, are modified. Isothermal treatments at 780 °C are accompanied by changes in the precipitation state of carbides / carbonitrides and simultaneous changes in the composition and defect density of the martensite matrix, depending on the time of treatment [32]. But notwithstanding this evidence, from the data obtained in the present analysis it is impossible to find a metallurgically justifiable relationship between the time of previous tempering and transformation temperatures. In view of this, we can only tentatively conclude that the effect of qualitative alteration of the chemical composition of austenite in the two steels because of the previous treatment at 780 ºC is strongly suggested.

4.1.2 Thermodynamic equilibrium calculations vs. non-equilibrium heating

In order to estimate the change of the equilibrium amount of MX and $M_{23}C_6$ precipitates with increasing temperature from 780 °C, a calculation by MTDATA [36] was carried out. The base composition used in the calculation was the corresponding to T91 steel (see Table 1). The equilibrium amount of precipitates and the fraction of constituents in the MX phase calculated by

MTDATA are shown in Figure 12. In this figure it is also shown the thermodynamic temperature at which full austenite is obtained under equilibrium conditions. It is worth noting that A_{c3} is always higher than A_{e3}. As shown in Figure 12, MX are almost all nitrides in the calculation; however, a minor fraction of Nb-rich carbides is also present.

In this point, it is interesting to mention that some controversy seems to exist in the previous literature about the chemical nature of the MX particles present at austenite temperatures in the range of 1050-1060 ºC. As shown, in this work only high-Nb precipitated particles are detected after 30 min. austenite holding time; other reports agree with the only presence of Nb-rich precipitates [40,41,42,43]. However, experimental evidence has also been presented as for the presence of V-containing precipitates (wt. % V~50 % and higher) in T91 steel samples normalized 10 min. at 1050 and 1100 ºC [44], and V-rich precipitates (wt. % V~80 %) in experimental Fe-Nb-V-C-N alloys austenitized at 1000 ºC or higher temperatures for several hundred hours [45].

4.1.3 A possible influence of the heating rate to austenite on further austenite grain growth

So far it has been described the theoretical evolution of $M_{23}C_6$ carbides and MX carbonitrides according with thermodynamic calculations. It is worth noting that Figure 12(b) seems to predict a V enrichment in MX precipitates for temperatures close to 780 °C (tempering temperature); on the other hand, the V content of the Type II (V-rich) MX precipitates (which are the major MX's) has been shown to increase only slightly with the time of treatment at 780 ºC at the expense of the Cr content[32]. This apparent increase must, however, be cautiously judged due to the experimental error of EDS quantification and possible artifacts due to the overlapping of the Cr-Kβ and V-Kα spectral lines. At the same time, EDS examination gave also some indications pointing to the fact that the coarser the MX precipitate, the richer in V it is [32].

The pinning action that inhibits austenite grain boundaries during austenite holding -thus keeping the austenite grain size at small values- is exerted by fine MX particles, which are mostly, according to our measurements at the end of the austenite holding time, Nb-rich. Such pinning particles may come, in principle, from only three sources, i.e. either they remain from the tempering step (these would be a minor group since they constitute a minor fraction of the MX population

during tempering [32]) or they nucleate and grow in the austenitizing step by combining the available Nb with the C released by dissolution of $M_{23}C_6$ precipitates, or they are formed from V-rich precipitates (that contain also non-negligible Nb amounts [32]) that release V during the heating ramp or austenite holding. In turn, the Nb needed to form Nb-rich MX particles in the second hypothesis may come either from solute Nb remaining from the tempering step or from the Nb bounded to V-rich MX precipitates if these last particles are dissolved during austenitization.

Since it has been reported in other works [46] that the increase in V content in MX precipitates leads to a decrease in their solubility temperature, one might propose that, if V_H is slow enough, i.e. 1 °C/s, *V-rich* MX and a major fraction of $M_{23}C_6$ precipitates could be dissolved during heating, thus releasing the *Nb* and C needed for a rapid nucleation of pinning particles. This could be true not only for short tempering times (that will keep the MX particle size relatively small) but also for the longer ones, because after long tempering times at 780 °C, MX precipitates, even becoming coarserwill slightly enrich in V [32], which might lower their dissolution temperature .

Increasing the heating rate up to 50 °C/s would change dramatically the scenario. At this high heating rate, the dissolution of a significant fraction of V-rich MX and $M_{23}C_6$ particles is deferred to high temperatures and will be, as already mentioned, completed during austenite holding, leading to a late precipitation of small Nb-rich, stable pinning particles, or at least to a fraction not enough to promote efficient pinning. This could increase the probability for heterogeneous austenite grain growth to occur. As an additional argument supporting the delayed dissolution of the $M_{23}C_6$ carbides, it is worth to mention that *isothermal* equilibrium dissolution of $M_{23}C_6$ in T91-type steel has been computationally simulated using the DICTRA software package, and the obtained result indicated an approximated time of 1000 seconds for a complete dissolution at 950 °C [47].

At the intermediate heating rate of 30 ºC/s, the initial metallurgical state has been shown to play a main role in the occurrence of heterogeneous growth (see Table 2). The precipitation of stable Nb-rich pinning carbides could still be delayed to the late stages of austenite holding; however, if the previous tempering time is long enough, V-rich MX particles and $M_{23}C_6$ particles will coarsen during tempering and could play a role on pinning *during its dissolution*, i.e., there could be a *transient pinning* action. In other words, the coarser particles formed during long-term tempering could attain a size appropriate to pin grain boundaries within an intermediate stage of their dissolution.

The hypothesis of transient pinning could, of course, be also valid for the 50 ºC/s heating rate; however, austenite grain growth after heating at this rate was observed to be always heterogeneous, that is, insensitive to the time of previous tempering, although *the area fraction of abnormally grown grains seems to diminish with the increase of previous tempering time*. This last result suggests that heterogeneous grain growth would be inhibited even after heating at 50 ºC/s if the time of previous tempering is increased long enough.

Finally, another factor related to the heating rate and playing a role on triggering heterogeneous austenite grain growth could be looked for in the relationship between the initial austenite grain size distribution, that is, the size distribution at the very start of austenite holding, and the pinning particle size distribution at the same time. Heating at higher rates changes the temperature range at which austenite is formed, and changes also the density of austenite nuclei. In principle, the higher the heating rate, the more the martensite defect network (dislocations, boundaries of different type, $M_{23}C_6$ precipitates) is "retained" up to high temperature and hence, the higher the density of austenite nucleation sites is, giving an austenite initial grain size smaller, that is, a microstructure that would be more prone to suffer heterogeneous grain growth. Indeed, a thorough study of Rios [48] has pointed out that the microstructure most susceptible to abnormal grain growth would consist of very fine grains pinned by very fine fairly slowly coarsening particles.

4.2 Two-step austenite transformation regime as recorded by dilatometry

With respect to the change in slope detected in the dilatometric curve during heating from the as-received condition in both T91 and T9 steels (Figure 7), it is worth mentioning that highly sensitive equipment such as the dilatometer used in this work is able to detect slight changes in the kinetics of austenite formation during heating. The as-received microstructure of both steels (i.e, the starting microstructure for the heating cycles shown in Figure 1) consists, as already mentioned, in lath, tempered martensite (that we can call α') with presence of $M_{23}C_6$ and MX-type carbides. Due to the low carbon content of the steel, the bct tempered matrix is not very different from a bcc ferrite one.

The nucleation of austenite in a martensite, or tempered martensite matrix has not been exhaustively analyzed in the previous literature; however, some reports account for its main

features. Thus, Law and Edmonds [49] studied the austenite formation from martensite and bainite in a Fe-1% V-0,2% C steel. They found that at low austenitization temperatures within the intercritical region, austenite nucleated at former austenite grain boundaries and, to a lesser extent, along lath boundaries within the former austenite grains. Increasing the austenitizing temperature produced a change in the preferred nucleation sites, the intragranular ones becoming more important. Similar results were reported by por Matsuda et al. [50] in a Fe-0,12% C-3.5% Ni steel, and Tokizane et al. [51] in a Fe-0,2% C steel. Thus, these results suggest that there could be a change not only in the austenite nucleation rate but also in the activation of different austenite nucleation sites as temperature increases, which would manifest itself as a change in austenite formation kinetics.

In addition, Wang et al. [52] proposed recently that the austenitization process in samples of a P92 ferritic-martensitic steel -that is, a steel very similar to ours- consists in a transformation step from α to γ around carbide particles and a further homogenization process with the dissolution of retained carbides and/or redistribution of Cr from Cr-enriched regions upon heating.

According to Wang's proposal, with increasing temperature above the onset temperature for austenite transformation, more and more austenite phase will form a first constituent (that we can call γ1) enclosing carbides. Eventually, a transient suppression or slowing down of the transformation might result if the austenite phase enveloping the carbides is thick enough, due to the slower diffusion kinetics of alloy elements in austenite than in ferrite [53,54]. The transformation will restart at a higher temperature by forming a second austenite constituent γ2, when both the diffusion kinetics and the driving force to form more austenite are enhanced. In the same line of reasoning as Wang's for austenite formation, Shtansky et al. [55] observed in a Fe–8.2Cr–C ferritic steel with spheroidized alloy carbides that the austenite first nucleates at α/α grain boundary triple points in the vicinity of Cr-enriched carbides or directly in contact with carbides located on the α/α grain boundaries, and that the kinetics of austenite growth appear to be controlled by Cr diffusion, the diffusion of C being much faster.

Thus, it is conceivable to consider Wang's picture for austenite formation as a basis to explain the change of slope we observed in our experiments at high heating rate (30 and 50 ºC/s). Indeed, at those rates the time elapsed within the lower intercritical region (that is, the temperature region up

to the change of slope of the dilatometric record) would be not enough for the complete diffusion of the Cr coming from $M_{23}C_6$ carbide dissolution. Moreover, as mentioned in the last section, a significant fraction of the $M_{23}C_6$ particles could be dissolved only after having attained the austenite holding temperature (1050 ºC), making it necessary the activation of other nucleation sites for austenite (interfaces not close to carbides, “retained” dislocation networks, etc.). These facts would be reflected in the described change in austenite formation kinetics. On the contrary, at the “low” heating rate (1 ºC/s), $M_{23}C_6$ carbide dissolution and subsequent Cr diffusion could cope with a “continuous” austenite nucleation and growth process.

Finally, the increasing trend observed for the A_{c1} temperature as a function of the time of previous treatment at 780 ºC (Figure 9) could be due to a diminution of the potential austenite nucleation sites; this diminution would be the result of both the coarsening of carbides [32] (with an associated decrease of their number density) and the coarsening of the microstructure itself (with a similar decrease in the number density of dislocations and martensite interfaces).

4. Conclusions

The experimental results obtained in the present work show that the occurrence of heterogeneous austenite grain growth during austenitizing at fixed temperature and holding time is a function of the heating rate to austenite and the starting metallurgical condition for the ASTM A213 - T91 steel. High heating rates and short tempering times favor the growth of a few abnormal grains in a matrix of uniform, small-sized grains. On the opposite, homogeneous austenite grain size distributions are obtained for low heating rates and long tempering times. The comparison between the behavior of the T91 and T9 steels (with and without, respectively, the stabilizing alloying elements Nb and V) shows that, for a fixed initial metallurgical state, heating at rates high enough is a necessary but not sufficient condition for the occurrence of such a heterogeneous grain growth. The absence of abnormal grain growth in the Nb/V-free T9 steel for the same experimental conditions demonstrates that Nb and/or V-rich particles play a major role in the heterogeneous austenite grain growth phenomenon. A threshold value of the heating rate to austenite seems to exist, from which on the dilatometric curve features would indicate a two-step austenite transformation process. In

the case of the T91 steel, the results show a correspondence between the occurrence of heterogeneous austenite grain growth and this possible two-step austenitizing process.

5. Acknowledgements

NZG, MIL and CAD acknowledge financial support of National Science and Technology Agency from Argentina in the form of PICT 2005 Nº 33325 contract. CC, CGDA and ITC acknowledge financial support of the Spanish Ministerio de Economia e Innovación in the form of a Coordinate Project (ENE2009-13766-C04-01) in the Energy Area of Plan Nacional 2009.

6. References

[1] T. Fujita, ISIJ Int. 32 (1992) 175.

[2] F. Masuyama, ISIJ Int. 41 (2001) 612.

[3] R. L. Klueh, Int. Mater. Rev., 50 (2005) 287.

[4] K. Maruyama, K. Sawada, J. I. Koike, ISIJ Int. 41 (2001) 641.

[5] H. Cerjak, P. Hofer, B. Schaffernak, ISIJ Int. 39 (1999) 874.

[6] R. K. Shiue, K. C. Lan, C. Chen, Mater. Sci. Eng. A A287 (2000) 10.

[7] C. Zener, Trans. AIME 175 (1948) 15.

[8] T. Gladman, F. B. Pickering, J. Iron Steel Inst. 205 (1967) 653.

[9] G. R. Speich, L. J. Cuddy, C. R. Gordon, A. J. DeArdo, Phase Transformations in Ferrous Alloys, TMS-AIME, Warrendale, PA, 1984.

[10] L. J. Cuddy, J. C. Raley, Metall. Trans. A, 14 (1983) 1989.

[11] A. P. Gulyaev, L. N. Serebrennikov, Metalloved. Term. Obrab. Metallov. 4 (1977) 2.

[12] D. Chakrabarti, C. L. Davis, M. Strangwood, Mater. Sci. Technol. 25 (2009) 939.

[13] A. Kundu, C. L. Davis, M. Strangwood, Sol. State Phen. 172-174 (2011) 458.

[14] G. Sheard, J. Nutting, Metal Sci. 13 (1979) 131.

[15] F. Peñalba, C. García de Andrés, M. Carsi, F. Zapirain, J. Mater. Sci. 31 (1996) 3847.

[16] A. Rossi, A. Mascanzoni, G. Crispoldi, F. de Meo, Proc. Fundamentals of Microalloying Forging Steels, The Met. Soc. of AIME, Warrendale, PA, 1987.

[17] T. Baker, Future Developments of Metals and Ceramics, Institute of Materials, London, 1992.

[18] D. San Martin, F. G. Caballero, C. Capdevila, C. García de Andrés, Mater. Trans. 45 (2004) 2797.

[19] J.C. Brachet, A. Alamo, Mém. Et. Sci. Rev. Mét. 87 (1990) 33.

[20] A. Danón, C. Servant, A. Alamo, J. C. Brachet, Mater. Sci. Eng. A, 348 (2003) 122.

[21] F. Abe, M. Tabuchi, S. Tsukamoto, Mater. Sci. Eng. – Energy 4 (2012) 166.

[22] C. García de Andrés, L.F. Álvarez, J. Mater. Sci. 28 (1993) 1264.

[23] O. P. Morozov, T. A. Popova, Phys. Met. Metall. 61 (1986) 100.

[24] C. García de Andrés, F.G. Caballero, C. Capdevila, L.F. Álvarez, Mater. Charact. 48 (2002) 101.

[25] ASTM Standard C33, Standard Test Methods for Determining Average Grain Size, ASTM International, West Conshohocken, PA, 2003.

[26] L.F. Álvarez, C.García, Rev. Metall – Paris 2 (1993) 245.

[27] F.G. Caballero, C. Capdevila, C. García de Andrés, ISIJ Inter 43 (2003) 726.

[28] D. San Martín, P.E.J. Rivera-Díaz-del-Castillo, C. García-de-Andrés, Scr. Mater. 58 (2008) 926.

[29] V. Gaffard, A. F. Gourgues-Lorenzon, J. Besson, ISIJ Int. 45 (2005) 1915.

[30] D. San Martín, T. De Cock, A. García-Junceda, F. G. Caballero, C. Capdevila, C. García-de Andrés, Mater. Sci. Technol. 24 (2008) 266.

[31] B. Jeya Ganesh, S. Raju, A. Kumar Rai, E. Mohandas, M. Vijayalakshmi, K. B. S. Rao, B. Raj, Mater. Sci. Technol. 27 (2011) 500.

[32] N. Zavaleta Gutiérrez, H. De Cicco, J. Marrero, C. A. Danón, M. I. Luppo, Mater. Sci. Eng. A 528 (2011) 4019.

[33] K. Tokuno, K. Hamada, R. Uemori, T. Takeda, K. Itoh, Scr. Metal. 25 (1991) 871.

[34] N. Zavaleta Gutiérrez, M. I. Luppo, C. A. Danón, ISIJ Inter. 47 (2007) 1178.

[35] B. C. Schaffernak, H. H. Cerjak, Calphad 25 (2001) 241.

[36] H. Davies, MTDATA—A Tool for Research and Development in Materials, National Physical Laboratory, Teddington, UK, 2003.

[37] K.W. Andrews, JISI 203 (1965) 721.

[38] C. Capdevila, C. García-Mateo, F. G. Caballero, C. García de Andrés, Mater. Sci. Eng. A 386 (2004) 354.

[39] C. Garcia-Mateo, C. Capdevila, F. G. Caballero, C. Garcia de Andres, J. Mater. Sci. 42 (2007) 5391.

[40] K. Tokuno, K. Hamada, T. Takeda, JOM 4 (1992) 25.

[41] H. D. Kim, I. S. Kim, ISIJ Int. 34 (1994) 198.

[42] K. Tokuno, K. Hamada, R. Uemori, T. Takeda, K. Itoh, Scr. Met. Mater. 25 (1991) 871.

[43] W. Jones, C. Hills, D. Polonis, Metall. Trans. A 22 (1991) 1049.

[44] M. Yoshino, Y. Mishima, Y. Toda, H. Kushima, K. Sawada, K. Kimura, ISIJ Int. 45 (2005) 107.

[45] K. Inoue, N. Ishikawa, I. Ohnuma, H. Ohtani, K. Ishida, ISIJ Int. 41 (2001) 175.

[46] M. Taneike, K. Sawada, F. Abe, Metall. Mater. Trans. A 35 (2004) 1255.

[47] Y. Saito, A. Matsuzaki, C. Shiga, Proc. 8th International Conference on Heat Treatment of Materials, The Iron and Steel Insitute, Kyoto, Japan, 1992.

[48] P. R. Ríos, Acta Mater. 45 (1997) 1785.

[49] N. C. Law, D. V. Edmonds, Metall. Trans. A 11 (1980) 33.

[50] S. Matsuda, Y. Okamura, Trans. ISIJ 14 (1974) 444.

[51] M. Tokizane, N. Matsumura, K. Tsuzaki, I. Tamura, Metall. Trans. A 13 (1982) 1379.

[52] L. M. Wang, Z. B. Wang, K. Lu, Acta Mater. 59 (2011) 3710.

[53] G. R. Speich, A. Szirmae, M. J. Richards, Trans. Metall. Soc. AIME 245 (1969) 1063.

[54] A. M. Huntz, P. Guiralde, M. Aucouturier, P. Lacombe, Mem. Sci. Rev. Metall. 66 (1969) 85.

[55] D. V. Shtansky, K. Nakai, Y. Ohmori, Z. Metallkd. 90 (1999) 25.

Table 1 Chemical composition of the V&M steels ASTM A213 – T91 and T9 (in weight %)

Steel	C	Si	Mn	P	S	Cr	Mo	Ni	Al	Nb	V	N
T91	0.11	0.28	0.48	0.018	0.002	8.28	0.93	0.11	0.015	0.07	0.21	0.045
T9	0.12	0.30	0.52	0.020	0.003	8.29	0.93					

Table 2: Austenite grain structure of the T91 steel resulting from thermal cycles in the specified conditions. The symbols * and ⊗ stand for homogeneous and heterogeneous respectively.

Heating Rate to Austenite / Tempering Time	1ºC/s	30 ºC/s	50 ºC/s
As-received	*	⊗	⊗
1 hour	*	⊗	⊗
2 hours	*	⊗	⊗
3 hours	*	⊗	⊗
4 hours	*	*	⊗
5 hours	*	*	⊗
6 hours	*	*	⊗

Figure Captions

Figure 1: Thermal cycle used for tempering and further austenitizing.

Figure 2: (a) Optical micrographs and (b) prior austenite grain size distribution corresponding to the T91 steel austenitized 30 minutes at 1050 ºC. Heating rate to austenite: 1 ºC/s, initial metallurgical condition: as received (homogeneous).

Figure 3: Optical micrographs and prior austenite grain size distributions corresponding to the T91 steel austenitized 30 minutes at 1050 ºC. Heating rate to austenite: 30 ºC/s, initial metallurgical condition: tempered at 780 ºC during (a) 1 hour (heterogeneous) and (b) 4 hours (homogeneous).

Figure 4: Optical micrographs and prior austenite grain size distributions corresponding to the T91 steel austenitized 30 minutes at 1050 ºC. Heating rate to austenite: 50 ºC/s, initial metallurgical condition: tempered at 780 ºC during (a) 1 hour (heterogeneous) and (b) 6.5 hours (heterogeneous).

Figure 5: (a) Optical micrographs and (b) prior austenite grain size distribution corresponding to the T9 steel austenitized 30 minutes at 1050 ºC. Heating rate to austenite: 1 ºC/s, initial metallurgical condition: as received (homogeneous).

Figure 6: (a) Optical micrographs and (b) prior austenite grain size distribution corresponding to the T9 steel austenitized 30 minutes at 1050 ºC. Heating rate to austenite: 30 ºC/s, initial metallurgical condition: as received (homogeneous).

Figure 7: Dilatometric curves for the tempered martensite-austenite transformation of the as-received microstructure as a function of the heating rate corresponding to the (a) T91 steel and (b) T9 steel.

Figure 8: Normalized dilatometric curves for the tempered martensite-austenite transformation of the T91 and T9 steel as a function of the time of tempering at 780 ºC. Heating rate to austenite of (a) 1, (b) 30 and (c) 50 ºC/s.

Figure 9: Transformation temperatures as a function of the tempering time for the T91 and T9 steels heated to the austenite phase field at (a)1, (b) 30 and (c) 50 ºC/s

Figure 10: TEM micrographs showing extractive replica of precipitates in T91 steel treated 6 hours at 780 ºC before (a) and after (b) the complete austenitization step.

Figure 11: Chemical composition of the MX precipitates after the indicated thermal cycle, expressed in a Cr-Nb-V ternary diagram of T91 steel samples. Martensite tempered during (a) 1 hour, (b) 2 hours, (c) 4 hours, (d) 5 hours and (e) 6 hours. Heating rate to austenite: 30 ºC/s

Figure 12: Theoretical calculations of evolution with temperature of (a) M23C6 and MX precipitates, and (b) distribution of elements in such precipitates. Calculations are performed with MTDATA and based on the T91 steel composition (see Table 1).

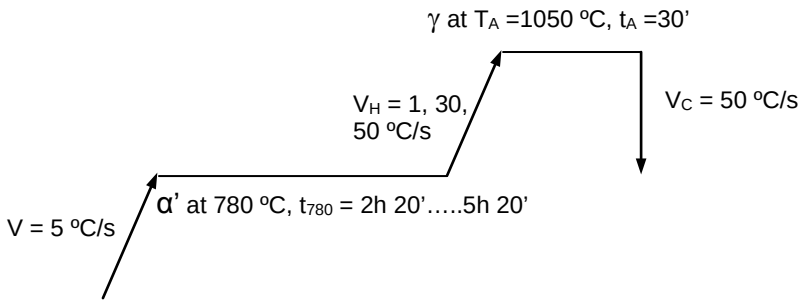

Figure 1: Thermal cycle used for tempering and further austenitizing.

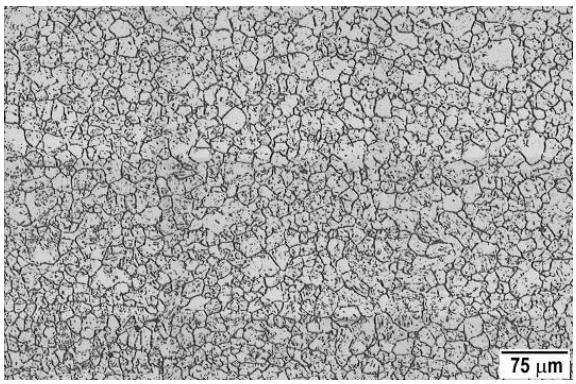

(a)

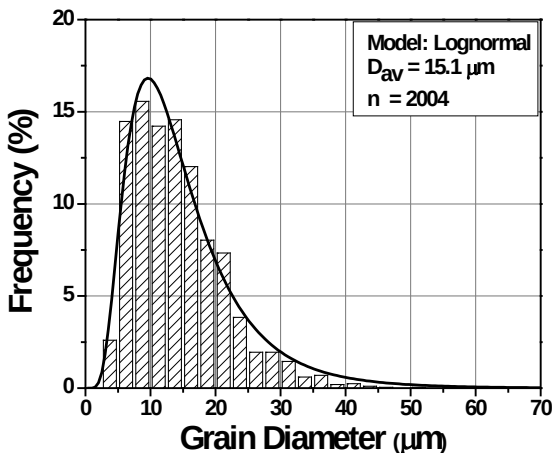

(b)

Figure 2: (a) Optical micrographs and (b) prior austenite grain size distribution corresponding to the T91 steel austenitized 30 minutes at 1050 ºC. Heating rate to austenite: 1 ºC/s, initial metallurgical condition: as received (homogeneous).

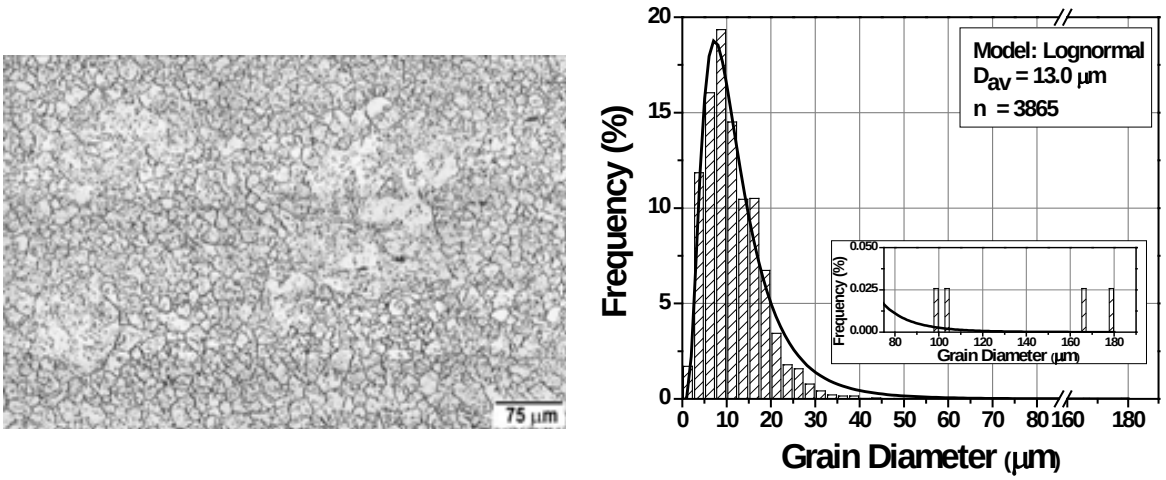

(a)

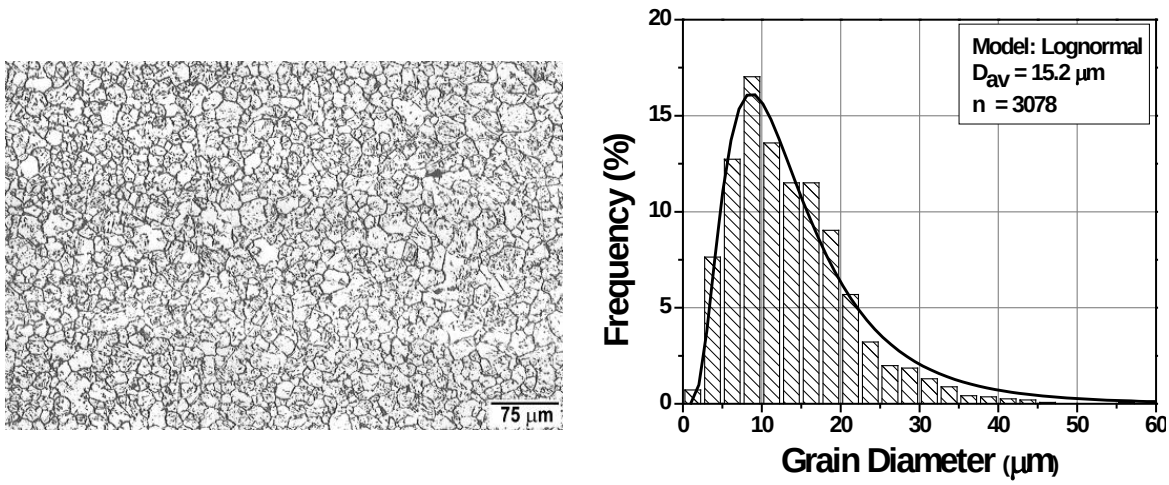

(b)

Figure 3: Optical micrographs and prior austenite grain size distributions corresponding to the T91 steel austenitized 30 minutes at 1050 ºC. Heating rate to austenite: 30 ºC/s, initial metallurgical condition: tempered at 780 ºC during (a) 1 hour (heterogeneous) and (b) 4 hours (homogeneous).

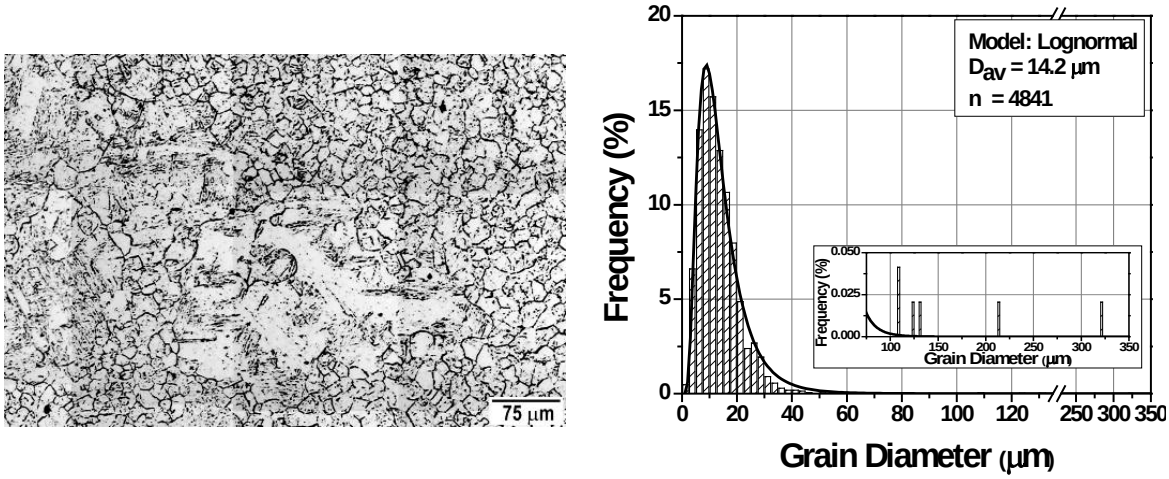

(a)

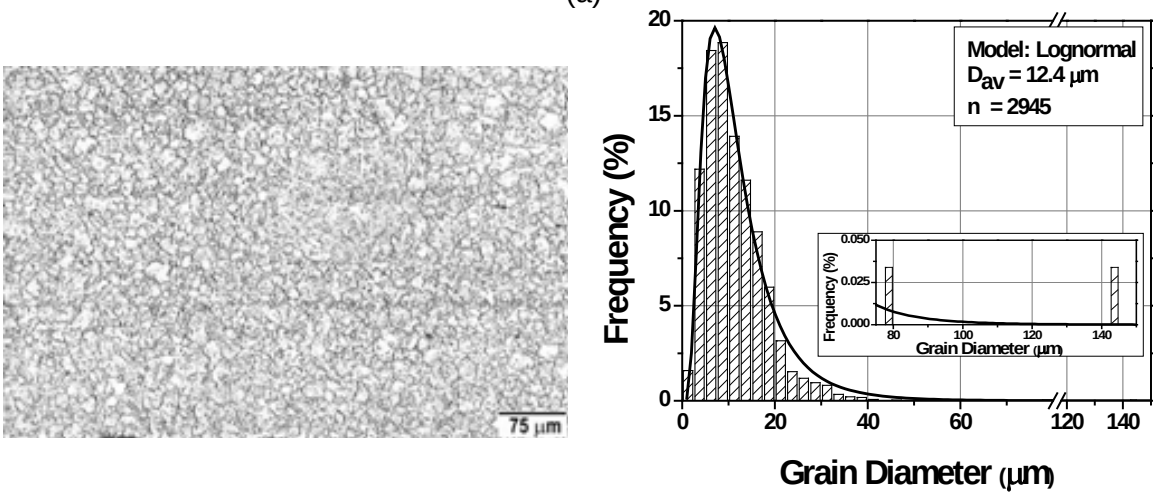

(b)

Figure 4: Optical micrographs and prior austenite grain size distributions corresponding to the T91 steel austenitized 30 minutes at 1050 ºC. Heating rate to austenite: 50 ºC/s, initial metallurgical condition: tempered at 780 ºC during (a) 1 hour (heterogeneous) and (b) 6.5 hours (heterogeneous).

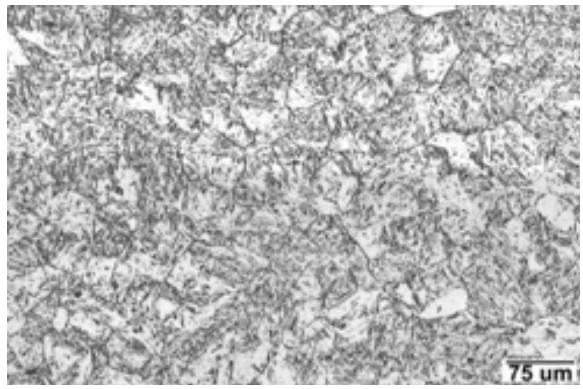

(a)

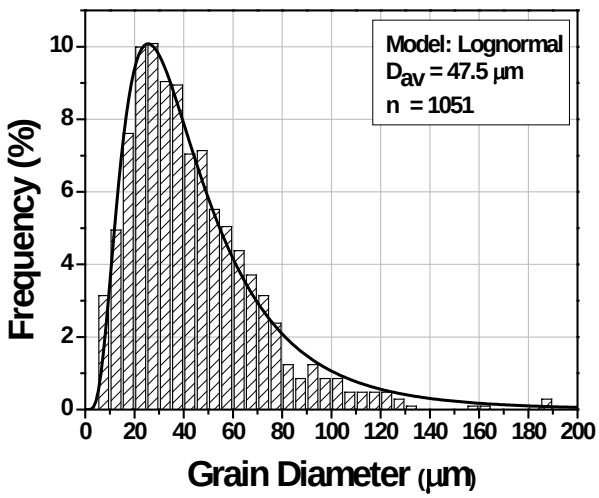

(b)

Figure 5: (a) Optical micrographs and (b) prior austenite grain size distribution corresponding to the T9 steel austenitized 30 minutes at 1050 ºC. Heating rate to austenite: 1 ºC/s, initial metallurgical condition: as received (homogeneous).

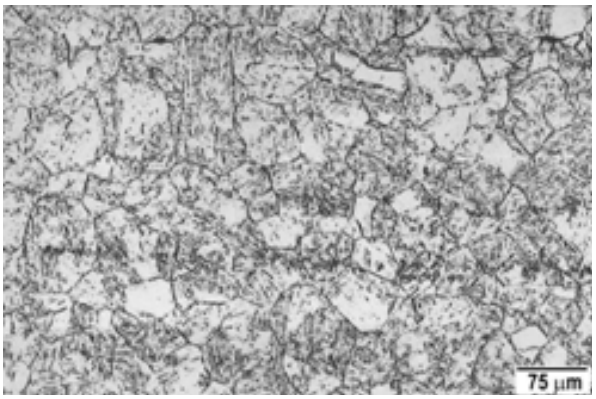

(a)

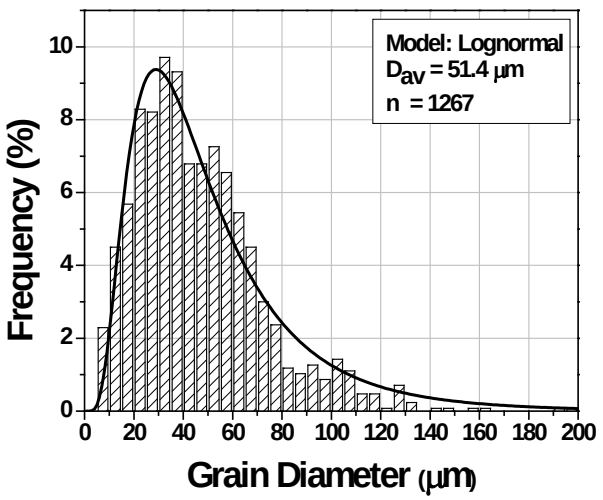

(b)

Figure 6: (a) Optical micrographs and (b) prior austenite grain size distribution corresponding to the T9 steel austenitized 30 minutes at 1050 ºC. Heating rate to austenite: 30 ºC/s, initial metallurgical condition: as received (homogeneous).

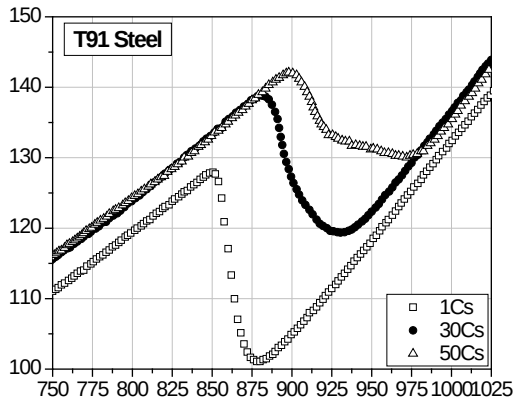

(a)

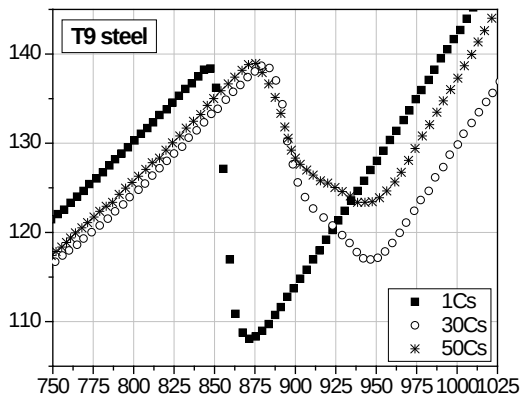

(b)

Figure 7: Dilatometric curves for the tempered martensite-austenite transformation of the as-received microstructure as a function of the heating rate corresponding to the (a) T91 steel and (b) T9 steel.

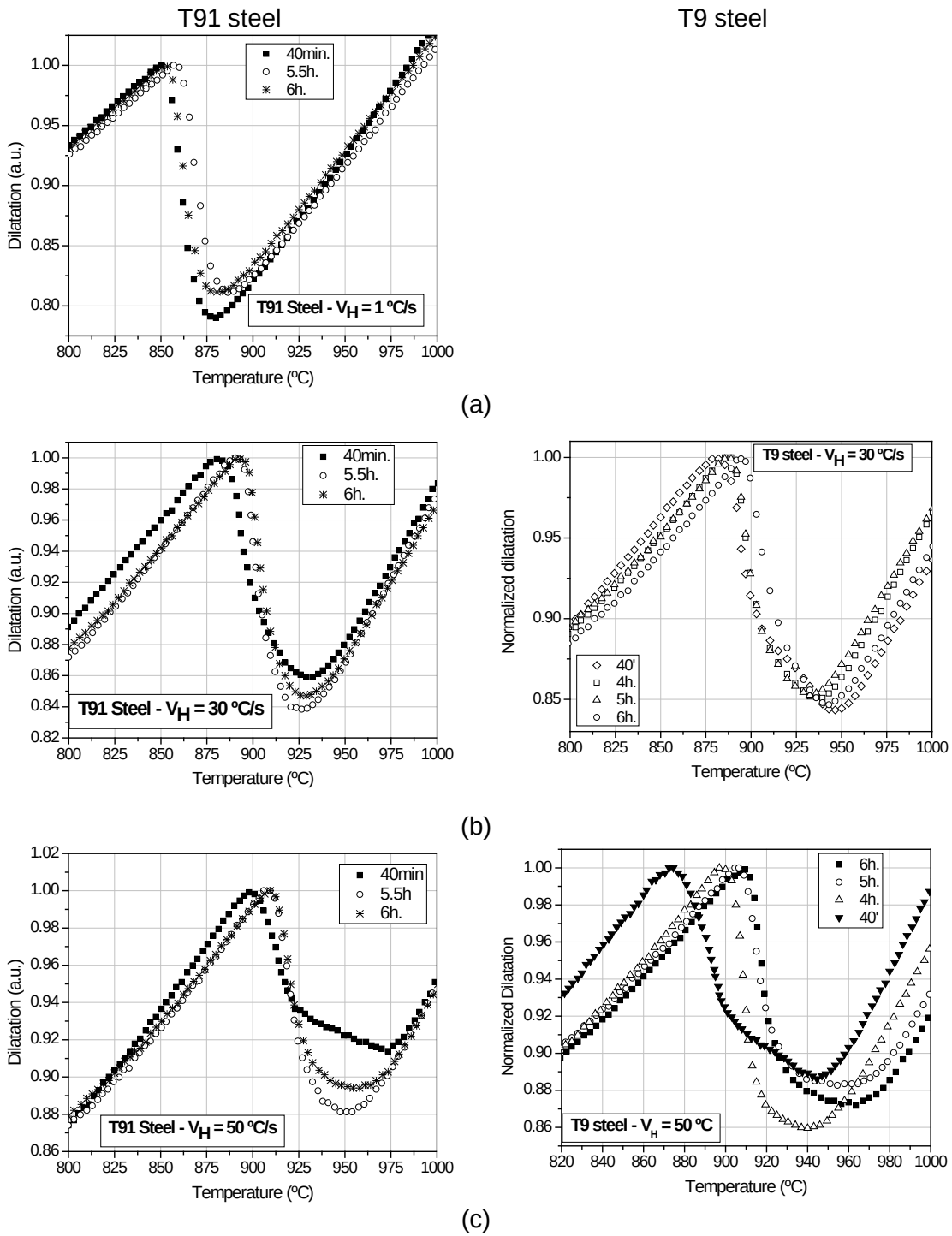

Figure 8: Normalized dilatometric curves for the tempered martensite-austenite transformation of the T91 and T9 steel as a function of the time of tempering at 780 ºC. Heating rate to austenite of (a) 1, (b) 30 and (c) 50 ºC/s.

T91 steel

T9 Steel

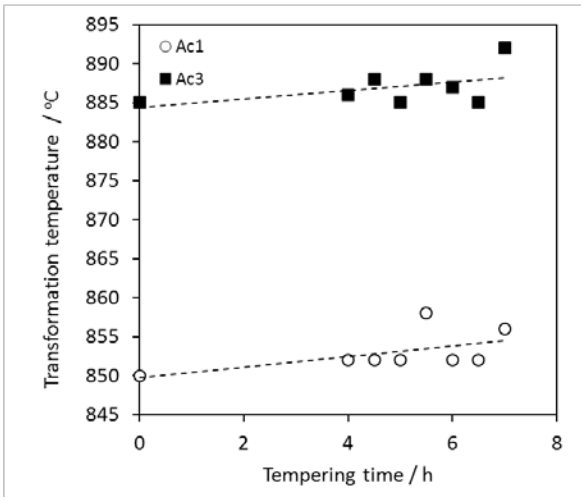

(a)

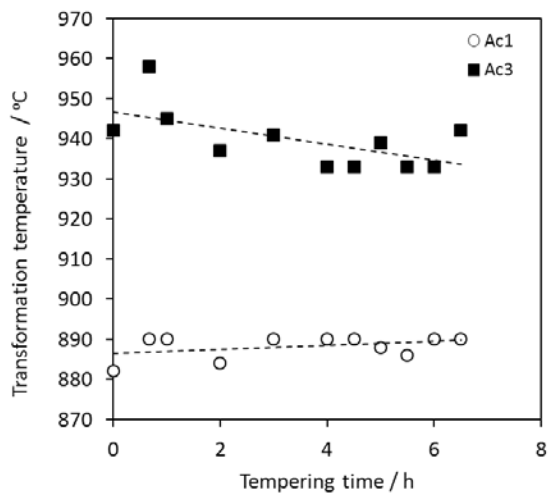

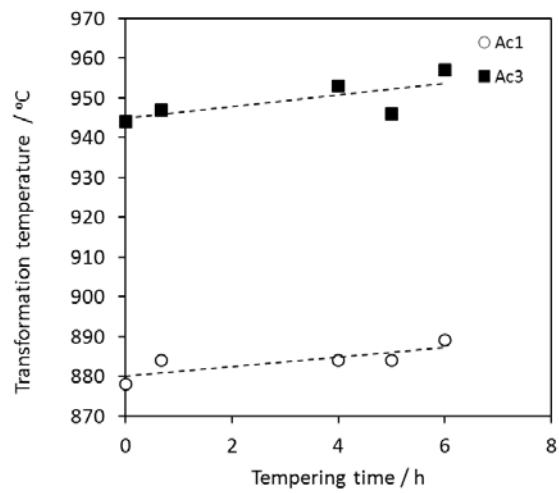

(b)

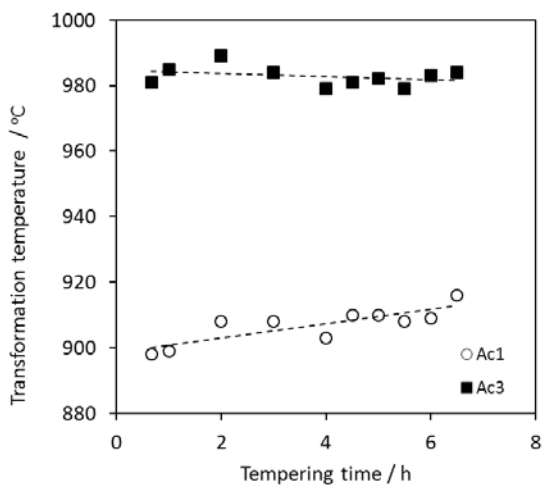

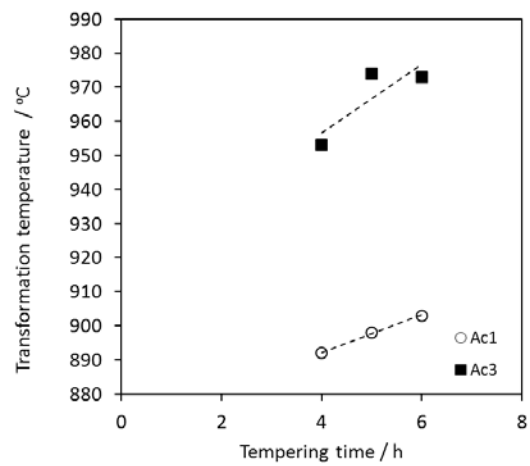

(c)

Figure 9: Transformation temperatures as a function of the tempering time for the T91 and T9 steels heated to the austenite phase field at (a)1, (b) 30 and (c) 50 ºC/s

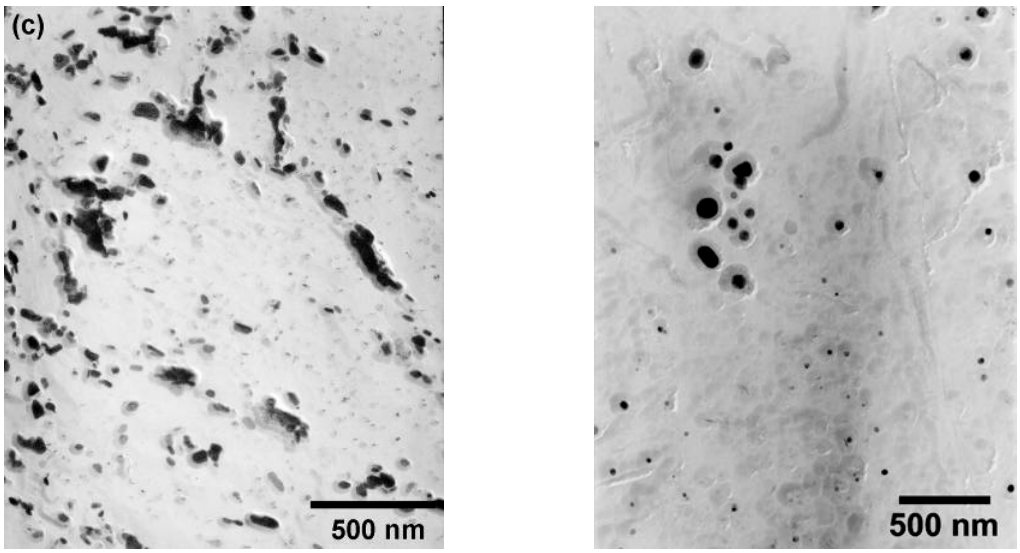

(a) (b)

Figure 10: TEM micrographs showing extractive replica of precipitates in T91 steel treated 6 hours at 780 ºC before (a) and after (b) the complete austenitization step.

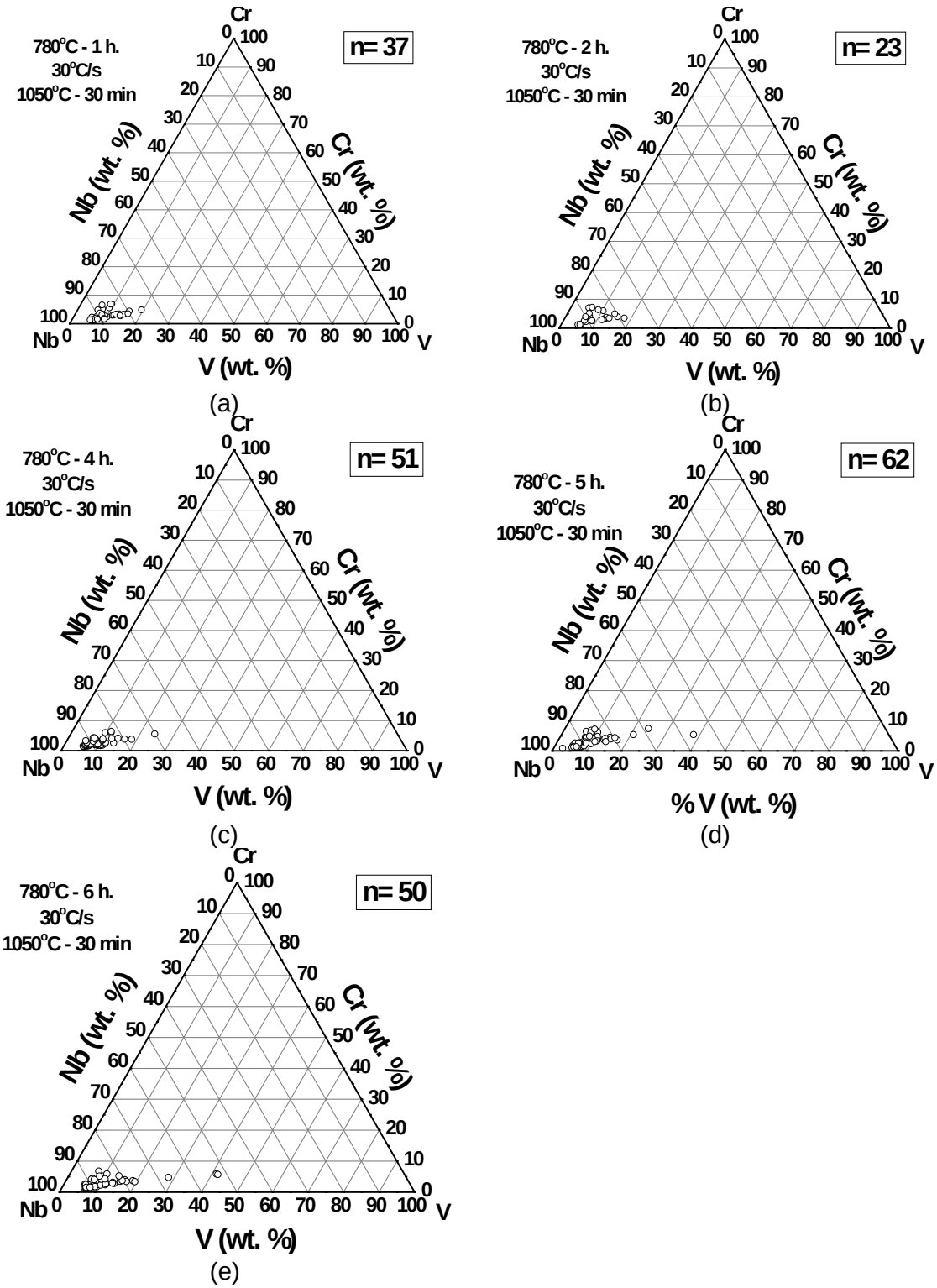

Figure 11: Chemical composition of the MX precipitates after the indicated thermal cycle, expressed in a Cr-Nb-V ternary diagram of T91 steel samples. Martensite tempered during (a) 1 hour, (b) 2 hours, (c) 4 hours, (d) 5 hours and (e) 6 hours. Heating rate to austenite: 30 ºC/s

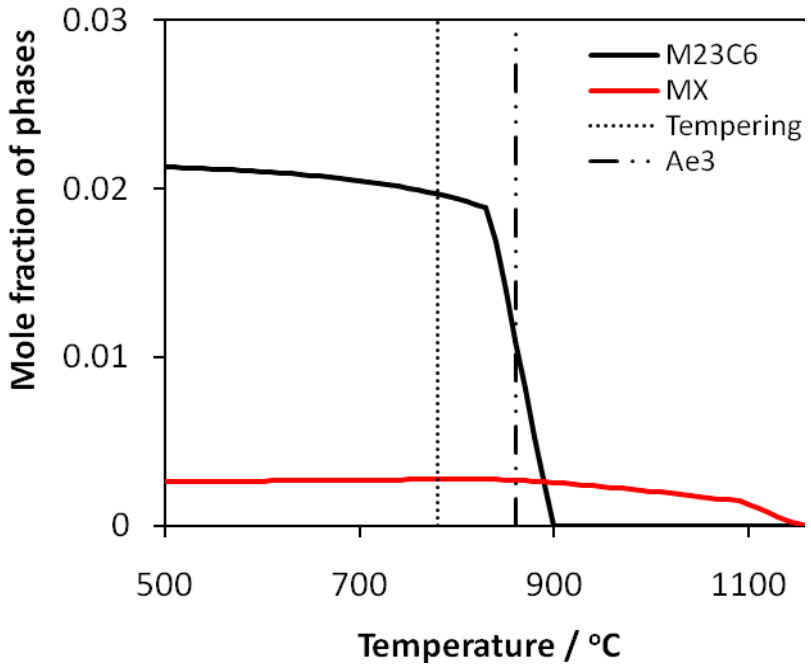

(a)

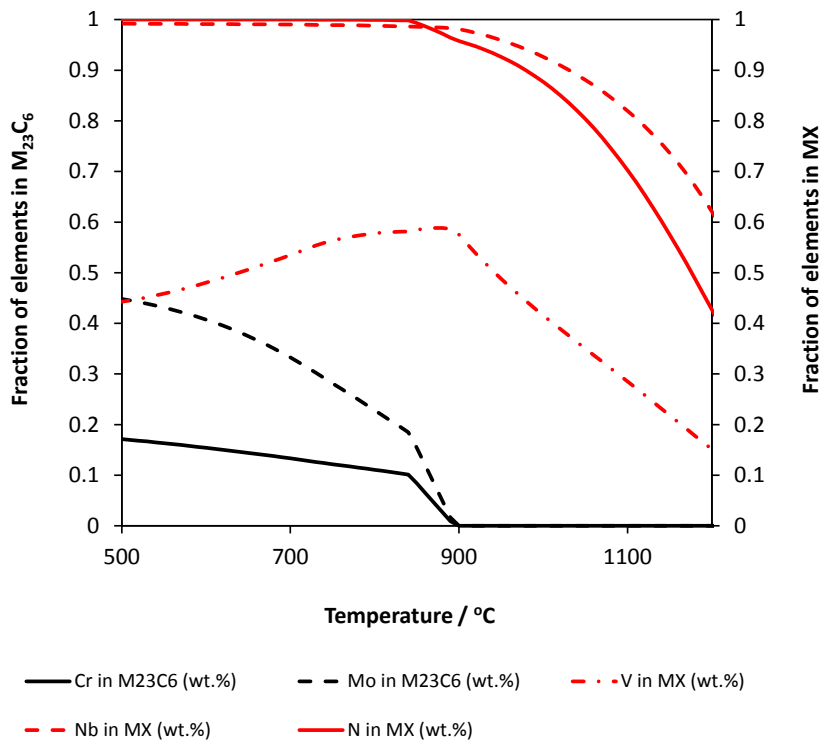

(b)

Figure 12: Theoretical calculations of evolution with temperature of (a) $M_{23}C_6$ and MX precipitates, and (b) distribution of elements in such precipitates. Calculations are performed with MTDATA and based on the T91 steel composition (see Table 1).